energies

MDPI

Article

Experimental Study on the Production Increase Mechanism of Supercritical Carbon Dioxide Fracturing in Coal-Rock Gas Reservoirs

Xiaodong Si *, Mian Zhang, Yan Gao, Hongxing Xu, Zefeng Li and Jiahui Yang

Changqing Downhole Technology Operating Company, CNPC Chuanqing Drilling Engineering Co., Ltd., Xi'an 710021, China; zhangmian@cnpc.com.cn (M.Z.); gaoyan029@cnpc.com.cn (Y.G.); cj_xuhongx@cnpc.com.cn (H.X.); cj_lizef@cnpc.com.cn (Z.L.); cj_yangjiah@cnpc.com.cn (J.Y.)
* Correspondence: sixiaodong0021@163.com

Abstract

China hosts abundant coal-rock gas (CRG) resources, which have become a critical unconventional natural gas contributor to national reserve expansion and production increment. Supercritical carbon dioxide ($ScCO_2$) fracturing is recognized as a green and efficient stimulation technology, exhibiting great potential for high-efficiency CRG exploitation. To clarify the effects and intrinsic mechanisms of $ScCO_2$ treatment on coal fracture initiation, propagation, and CRG recovery enhancement, true triaxial fracturing and CO_2-CH_4 displacement experiments were performed in combination with multiple microscopic characterization methods, including X-ray diffraction (XRD), Fourier-transform infrared spectroscopy (FTIR), and Scanning electron microscopy (SEM). The multi-scale experimental investigation systematically revealed the fracture development mechanism, permeability variation characteristics, and microstructural evolution of coal reservoirs under $ScCO_2$ interactions. The results indicate that $ScCO_2$ fracturing significantly lowers the coal fracture initiation threshold compared with conventional hydraulic fracturing, with the breakdown pressure reduced by 26.2% and the initiation time shortened by 37.5%. Such advantages facilitate coal fracture activation and the development of complex fracture networks. Long-term $ScCO_2$ soaking induces the dissolution of inorganic minerals (e.g., calcite, plagioclase, and clay minerals) and the extraction of inherent organic matter within coal matrices. The coupled hydro-chemical reactions reconstruct the coal pore structure, enlarge pore throats, and improve reservoir permeability, achieving a maximum permeability enhancement of approximately 1.6 times. Meanwhile, $ScCO_2$ displacement yields a prominent CRG recovery performance, with an ultimate gas recovery factor up to 93.85%. The CRG enhancement mechanism of $ScCO_2$ fracturing is comprehensively attributed to three core coupled effects. First, $ScCO_2$ dynamic fracturing generates intricate fracture networks, which greatly optimize reservoir seepage channels and flow space. Second, the $ScCO_2$–formation water–coal interaction modifies coal physical properties via mineral dissolution and organic matter extraction, thereby improving reservoir permeability. Third, the preferential adsorption of CO_2 over CH_4 triggers effective competitive adsorption and gas displacement, further promoting adsorbed methane desorption and elevating CRG recovery efficiency. This study provides a solid theoretical foundation for the field application of $ScCO_2$ fracturing technology and offers valuable insights into the green, efficient, and sustainable development of deep coal-rock gas resources.

Check for updates

Academic Editor: Alberto Maria Gambelli

Received: 15 June 2026
Revised: 14 July 2026
Accepted: 15 July 2026
Published: 17 July 2026

Copyright: © 2026 by the authors. Licensee MDPI, Basel, Switzerland. This article is an open access article distributed under the terms and conditions of the Creative Commons Attribution (CC BY) license.

Keywords: coal-rock gas; supercritical carbon dioxide; fracture propagation; soaking duration; pore and permeability; enhanced gas recovery

1. Introduction

In recent years, deep coalbed methane (located at depths exceeding 1500 m) has become widely known as "coal-rock gas" in China [1–3]. China hosts abundant coal-rock gas (CRG) resources with total reserves exceeding 30×10^{12} m^3, demonstrating considerable resource potential [4]. Similar to shale gas, CRG occurs within coal reservoirs in both free and adsorbed phases [5,6]. Since 2021, remarkable progress has been made in the exploration and commercial development of CRG in major petroliferous basins of China, including the Ordos, Junggar, and Sichuan Basins [7–9]. CRG is predominantly preserved in the adsorbed state within coal pore systems. Coal reservoirs are generally characterized by low porosity and low permeability, which poses substantial challenges for efficient gas exploitation. Current field development primarily adopts the multi-stage horizontal well fracturing technique, maturely applied in shale oil and gas exploitation, to improve coal reservoir permeability and ultimately enhance CRG productivity [10]. The large-scale deployment of conventional hydraulic fracturing in CRG reservoirs is restricted by two critical technical and environmental challenges. From the perspective of water resource utilization, the massive water consumption of hydraulic fracturing cannot be sustainably guaranteed in water-deficient regions, where the growing demand for fracturing water severely limits long-term field implementation [11,12]. From the reservoir protection perspective, coal exhibits strong gas adsorption affinity, and the extensive infiltration of water-based fracturing fluids inevitably induces severe formation damage [13,14]. Furthermore, the low-cost treatment and recycled utilization of flowback water still pose prominent technical difficulties [15].

In recent years, against the dual background of water conservation, carbon emission reduction and efficient reservoir stimulation, CO_2, as an eco-friendly fracturing medium, possesses unique technical and environmental advantages for CRG reservoir fracturing and production increase [16–19]. Yang et al. [20] established a new numerical model for predicting the wellbore temperature and pressure during supercritical CO_2 fracturing based on thermodynamics, heat transfer, fluid mechanics, and a numerical solution method. Wang et al. [21] carried out a true triaxial Supercritical carbon dioxide ($ScCO_2$) fracturing simulation and analyzed the pore morphology and structure variations in coal to investigate this transformation effects of fracturing parameters and stress conditions on the multi-scale pores. The effective transformation of pores induced by $ScCO_2$ fracturing can enable the smooth desorption and migration of coalbed methane in the low permeability reservoir, which creates the necessary conditions for its long-term and efficient extraction. Leng et al. [22] systematically investigated the pore-fracture architecture of deep coal seams in the JiaTan block of the Ordos Basin using an integrated suite of advanced techniques. The results reveal that enhancing methane desorption in micropore-rich matrices and improving fracture connectivity are identified as key levers for optimizing CRG extraction. Wang et al. [23] used a triaxial fracturing system to perform $ScCO_2$ fracturing in coal and found that compared with hydraulic fracturing, $ScCO_2$ fracturing can significantly increase the fracture connectivity, tortuosity, roughness, and structural complexity. Pan et al. [24] examined the effects of $ScCO_2$ fracturing on coal reservoir pore modification by conducting true triaxial $ScCO_2$ fracturing experiments on high-rank coal samples under various stresses and injection rates. The results show a significant impact on coal pore modification, with a 59.85% increase in porosity, 60% increase in pore volume, 56% increase in pore throat

volume, and 47.5% increase in permeability. Ma et al. [25] demonstrated that CO_2-enhanced coalbed methane recovery offers a promising solution to address the dual challenges in energy security and environmental sustainability. Through asphalt model simulations and experimental validation, Torrik et al. [26] confirm that CO_2 exhibits a higher surface affinity toward asphalt. This characteristic enables CO_2 to displace coalbed methane effectively, thereby facilitating enhanced methane recovery and mitigating greenhouse gas emissions. Integrating the supercritical CO_2 adsorption model with machine learning approaches, Jeon et al. [27] quantitatively determine coal key physicochemical properties, including volatile matter content, fixed carbon content, and vitrinite reflectance. These parameters are essential for predicting the competitive adsorption behavior of CO_2 and CH_4 on coal matrices. Zhang et al. [28] introduced a pioneering, cross-disciplinary mathematical model, and quantified fracture roughness, incorporating it with gas flow dynamics under multifaceted field conditions in coalbeds. This research offers novel insights into fracture behavior quantification in coalbed methane extraction engineering.

Nevertheless, existing research on $ScCO_2$ fracturing, especially for deep coalbed gas reservoirs, remains insufficient. The fundamental mechanisms controlling fracture initiation and propagation in deep coal formations have not been fully clarified. In addition, previous studies generally treat fracturing modification and gas production enhancement as independent research objects, lacking systematic and integrated investigations that correlate fracture evolution with gas recovery performance. Furthermore, the time-dependent effects of CO_2 soaking duration on coal microstructural alteration and recovery improvement efficiency remain poorly understood. These unresolved issues necessitate further in-depth quantitative and mechanistic research. To fill the aforementioned research gaps, true triaxial fracturing tests and CO_2-CH_4 displacement experiments were performed, combined with multiple microscopic characterization approaches, including X-ray diffraction (XRD), Fourier-transform infrared spectroscopy (FTIR), and Scanning electron microscopy (SEM). Integrating macroscopic experimental observations and microscopic structural analysis, this study systematically investigates the fracture initiation and propagation mechanisms of deep coal reservoirs subjected to $ScCO_2$ treatment. The effects of $ScCO_2$ soaking duration on coal microstructural evolution and permeability modification are quantitatively clarified. The findings of this work aim to provide theoretical support and practical guidance for the efficient development of CRG resources via $ScCO_2$ fracturing technology.

2. Experimental Materials and Methods

2.1. True Triaxial Fracturing Equipment and Procedure

True triaxial $ScCO_2$ fracturing tests were performed on a self-developed physical simulation platform, as visualized in Figure 1. This experimental system consists of four core subsystems, including a CO_2 pressurization and regulation module, a constant-temperature control module, a true triaxial stress loading module, and a real-time data acquisition module. The platform is capable of implementing fracturing tests under precisely controlled in situ stress, temperature and fluid injection rate conditions, and can continuously monitor the dynamic variation in injection pressure throughout the coal fracturing process in real time.

Cube coal specimens with a uniform dimension of 200 mm × 200 mm × 200 mm were adopted in all tests. A central borehole with a diameter of 10 mm and a depth of 120 mm was drilled vertically to the bedding plane on the top surface of each coal specimen. A steel pipe with an outer diameter of 8 mm was embedded into the borehole to a penetration depth of 100 mm, reserving a 20 mm hollow cavity at the borehole bottom as the initiation position for fracturing crack propagation.

All fracturing experiments were conducted under a predefined in situ stress regime, where the vertical stress (σ_v), maximum horizontal principal stress (σ_H), and minimum horizontal principal stress (σ_h) were set as 12 MPa, 14 MPa, and 10 MPa, respectively. A constant fluid injection rate of 20 mL/min was applied during the tests. Two types of fracturing fluids, i.e., conventional guar gum fracturing fluid and $ScCO_2$ fluid, were comparatively investigated, and the injection temperature of all fracturing fluids was stably maintained at 50 °C throughout the experimental procedure. Triplicate replicates of both experimental schemes were conducted under consistent thermal and stress fields to minimize stochastic operational uncertainties. Owing to the limited geometric volume of laboratory coal specimens, fluid injection triggers sharp, rapid pressure fluctuations within the sample assembly. Accordingly, the entire fracturing test sequence is generally finalized within several minutes.

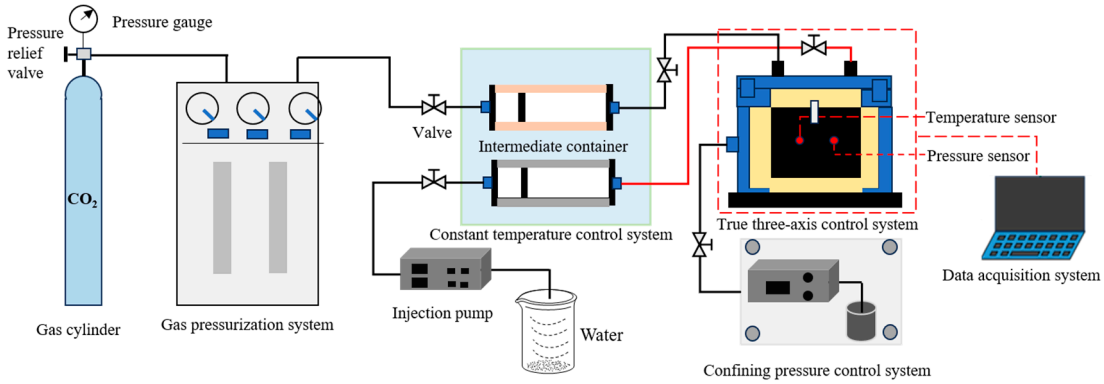


Figure 1. Schematic diagram of the physical simulation platform for true triaxial fracturing.

2.2. CO_2-Enhanced CRG Recovery Experiments

CO_2-enhanced CRG recovery experiments were carried out on a self-developed flow displacement experimental apparatus (Figure 2). The experimental system is composed of seven functional modules, including a gas supply module, a gas pressurization module, a confining pressure loading module, a core holder, a back-pressure control module, a gas measurement and collection module, and a data acquisition module. During the gas injection process, the gas permeability of coal cores was determined based on the average gas flow rate in accordance with Darcy's law, as defined in Equation (1).

$$k = \frac{\mu L \overline{Q}}{(P_1 - P_2)A} = \frac{2\mu Q P_\alpha L}{(P_1^2 - P_2^2)A} \quad (1)$$

where P_1 and P_2 represent the inlet and outlet pressures at both ends of the coal core (MPa); $\overline{Q}$ denotes the average outlet gas flow rate (mL); k is the fluid permeability of the coal core (10^{-3} μm^2); μ refers to the dynamic viscosity of the test fluid (Pa·s); Q is the fluid flow rate (mL); P_α is the standard atmospheric pressure, which is fixed at 0.1 MPa; L and A correspond to the length (cm) and cross-sectional area (cm^2) of the coal core specimen, respectively. During the experiment, gas was continuously injected into coal-rock specimens to conduct competitive displacement over a minimum duration of 4 h. Once the injection pressure and effluent gas flow rate attained a steady equilibrium state, experimental data were logged, and matrix permeability was subsequently quantified via the derived theoretical formula. Triplicate replicates of all experimental schemes were conducted under consistent experimental conditions to minimize stochastic operational uncertainties.

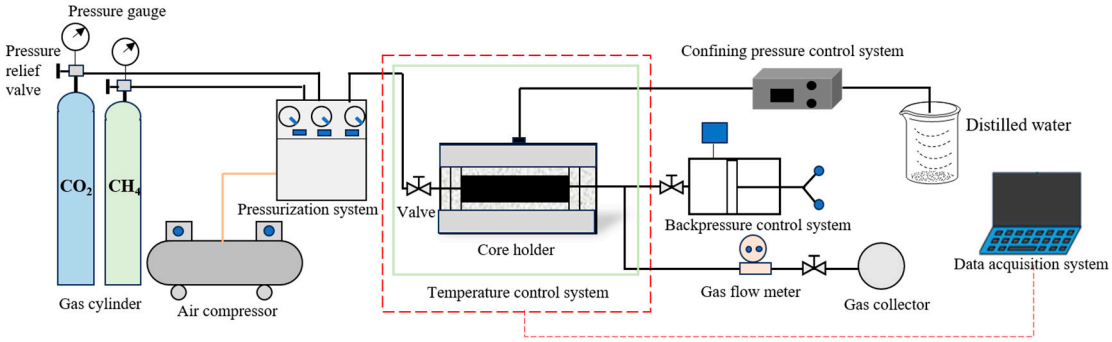


Figure 2. Schematic diagram of the CO_2-Enhanced CRG Recovery experimental system.

The overall experimental procedure is divided into two main stages; namely, coal-rock core pretreatment and CO_2 displacement of CRG tests on treated coal cores.

$ScCO_2$ soaking pretreatment. Prior to the displacement tests, coal core specimens were first saturated with formation water, followed by continuous CO_2 injection. The core holder was fully sealed to construct a coupled CO_2–formation water–coal reaction environment. The reaction temperature and pressure were maintained at 85 °C and 8 MPa, respectively. Four different CO_2 soaking durations were designed, including 0 d (blank control group without CO_2 injection), 5 d, 10 d, and 15 d. After the completion of CO_2 reaction and soaking, all cores were vacuum-dried for subsequent experiments.

CO_2-CH_4 displacement experiments. The detailed experimental procedures are specified as below:

① The pretreated coal-rock core was placed into the core holder, and the confining pressure was gradually elevated to 8 MPa. The outlet valve was closed, and the core was vacuumized for 6 h using a vacuum pump to eliminate residual gas and impurities inside the core.

② The inlet valve was opened to inject pure CH_4 into the core. After the back-pressure and outlet gas flow rate reached a stable state, continuous methane injection was performed for 24 h to achieve full CH_4 saturation of the coal-rock core.

③ The valve of the CO_2 cylinder was opened, and CO_2 was injected at a constant pressure of 8 MPa. The real-time outlet gas flow rate was continuously measured during the injection process. Meanwhile, produced gas samples were collected using gas sampling bags for component analysis, to quantify the recovered CH_4 volume and further calculate the CRG recovery efficiency. $ScCO_2$ was continuously injected into coal-rock specimens to displace adsorbed methane over a minimum duration of 6 h. The displacement process was regarded as fully accomplished once the CO_2 volume fraction measured at the effluent sampling outlet exceeded 99%. Triplicate replicates of all experimental schemes were conducted under consistent experimental conditions to minimize stochastic operational uncertainties.

④ Upon the termination of the experiment, the data acquisition system and CO_2 cylinder valve were closed sequentially. All the pressure was unloaded, both ends of the core holder were opened, and the coal-rock core specimen was removed for subsequent analysis.

Coal-rock core specimens investigated in this study were drilled from the No. 8 coal seam of the Benxi Formation in a typical block of the Ordos Basin. All core samples were processed to a uniform dimension of 5 cm in length and 2.5 cm in diameter. In addition, the tested coal specimens exhibit an intrinsic porosity about 8%, with an initial matrix permeability spanning around 0.12 mD. The proximate analysis results and basic physicochemical properties of the collected coal samples are summarized in Table 1. The formation water

utilized in the experiments was sampled from an in situ CRG well within the same study block, and its detailed ionic constituents and pH characteristics are presented in Table 2.

Table 1. Proximate analysis results of coal sample.

Samples	Vitrinite	Inertinite	Exinite	Mineral
No. 8 coal	80.6%	12.2%	0.7%	6.5%

Table 2. Ionic constituents and pH of formation water sample.

Ionic	Cl^-	Ba^{2+}	Fe^{2+}	Ca^{2+}	Na^+	Mg^{2+}	K^+	pH
Content (mg/L)	9.50×10^4	3.50×10^3	200	2.18×10^4	3.29×10^4	1.94×10^3	300	5.1

2.3. Microscopic Characterization of Coal-Rock Before and After Reaction

Mineral component variations in coal before and after the $ScCO_2$–formation water–coal interaction were quantitatively determined via XRD (D8 ADVANCE, Bruker AXS GmbH, Karlsruhe, Germany) tests. Prior to testing, coal samples were ground into fine powders with particle sizes smaller than 0.074 mm, and a fixed sample mass of 1 g was adopted for each test. The XRD Scanning procedure was performed over a 2θ range of 10–90°, with a step size of 0.2° and a Scanning rate of 8°/min.

FTIR tests were conducted on a spectrometer (VERTEX 80v, Bruker Corporation, Karlsruhe, Germany) to identify and analyze the organic functional group distributions of coal specimens. The spectra were recorded within the wavenumber range of 400–4000 cm^{-1} at a spectral resolution of 0.06 cm^{-1}. Consistently, coal powders with particle sizes below 0.074 mm were fully dried in advance. The conventional KBr pellet method was employed for sample preparation and subsequent spectral measurement.

The microstructural morphology and elemental composition of coal samples were characterized using a SEM (JSM-5800, JEOL, Akishima, Japan). For sample preparation, conductive adhesive tape was affixed to the sample stage, and thin coal sections were carefully mounted on the tape with tweezers. Surface dust and impurities were removed using a rubber suction bulb, and all samples were sputter-coated with a thin gold layer to enhance surface conductivity for high-resolution imaging. The prepared samples were then transferred into the SEM vacuum chamber for microscopic observation. All morphological observations were performed at an accelerating voltage of 10 kV. The instrument achieved a point resolution superior to 0.19 nm and a line resolution better than 0.1 nm.

3. Results and Discussion

3.1. Patterns of Fracture Propagation and Formation Mechanisms in Coal-Rock

Figure 3 illustrates the temporal evolution of injection pressure during $ScCO_2$ fracturing and conventional hydraulic fracturing, respectively. Based on the pressure response profiles in Figure 3, the $ScCO_2$ fracturing process can be classified into six distinct stages: rapid cavity filling, steady pressure build-up, accelerated pressure rise, abrupt pressure drop, stable pressure decline, and secondary rapid pressure reduction. In comparison, conventional hydraulic fracturing exhibits a simplified four-stage pressure evolution pattern, consisting of rapid pressure increase, slow sustained pressure elevation, sharp pressure drop, and secondary rapid pressure reduction.

Comparative experiments were conducted under identical in situ stress, temperature, and injection rate conditions. The results show that conventional hydraulic fracturing yields a coal breakdown pressure of 13.88 MPa with a breakdown time of 40 s, while $ScCO_2$ fracturing presents a considerably lower breakdown pressure of 10.24 MPa and a shorter

breakdown time of 25 s. Quantitatively, $ScCO_2$ fracturing reduces the coal-rock breakdown pressure by 26.2% and shortens the breakdown duration by 37.5% relative to conventional hydraulic fracturing. These findings demonstrate that $ScCO_2$ can effectively promote coal fracture initiation, which facilitates the development of complex fracture networks in coal reservoirs.

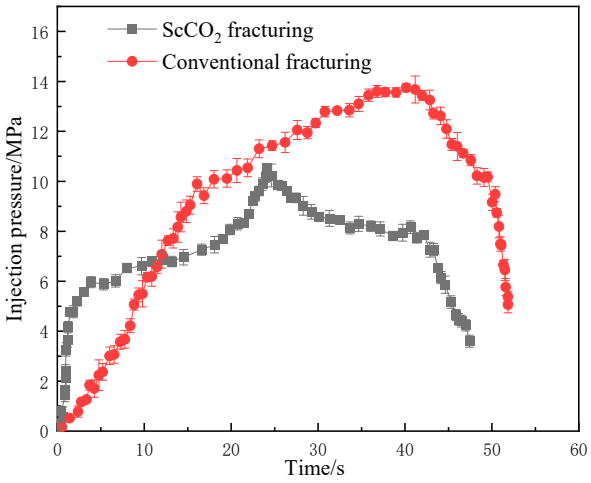


Figure 3. Time-dependent injection pressure curves in true triaxial fracturing.

Figure 4 presents the fracture morphologies of coal specimens fractured using different fracturing media. For conventional hydraulic fracturing (Figure 4a), only a single dominant fracture is formed with negligible secondary crack development, thereby producing a simple fracture system with low structural complexity. In comparison, $ScCO_2$ fracturing yields a distinctly different fracture pattern, as displayed in Figure 4b. Multiple primary fractures initiate from the injection borehole and propagate along divergent orientations, accompanied by abundant secondary microfractures, which contributes to a highly complicated fracture geometry. Consistent with the experimental observations, both hydraulic and $ScCO_2$ fracturing can generate penetrating main fractures on coal surfaces. Nevertheless, the fracture network induced by $ScCO_2$ fracturing exhibits a substantially higher degree of complexity compared with that formed via conventional hydraulic fracturing.

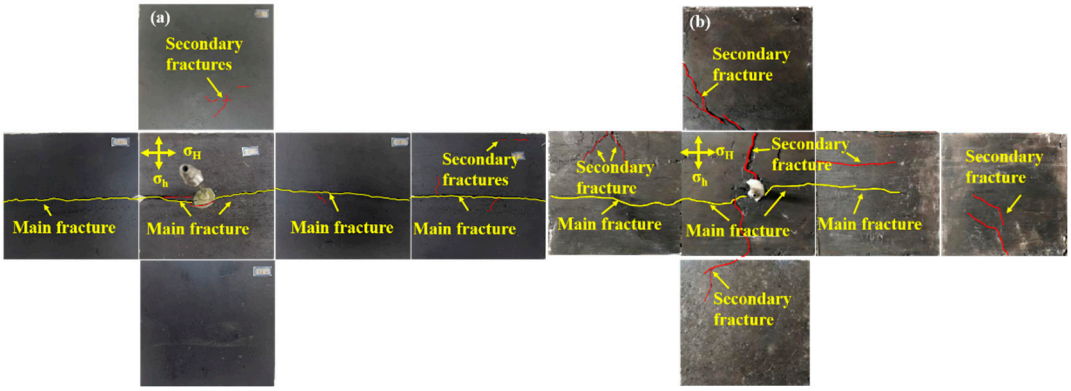


Figure 4. Fracture propagation under different fracturing fluids, (**a**) guar gum, (**b**) $ScCO_2$.

The temporal injection pressure curve of $ScCO_2$ fracturing in coal exhibits distinct nonlinear evolutionary characteristics, which can be divided into six sequential stages (Figure 5). ① Rapid cavity-filling stage: Owing to the superior diffusivity of CO_2, the borehole cavity is rapidly filled at the initial injection stage, triggering an abrupt pressure rise. This characteristic differs substantially from the gradual pressure increase observed in conventional hydraulic fracturing. ② Steady pressure build-up stage: In this stage,

CO_2 gradually penetrates the coal matrix pores and natural fractures. Benefiting from the high compressibility of CO_2 fluid, system pressure accumulates slowly and stably. ③ Accelerated pressure rise stage: Once the fluid pressure exceeds the critical threshold, CO_2 undergoes a subcritical-to-supercritical phase transition. The resultant drastic changes in fluid thermophysical properties induce a sharp pressure elevation before coal fracture initiation. ④ Rapid pressure drop stage: When the injection pressure reaches the ultimate breakdown threshold, coal rock ruptures. The high-pressure $ScCO_2$ fluid rapidly invades newly generated fractures, leading to an instantaneous drop in system pressure. ⑤ Stable pressure decline stage: Dynamic equilibrium is established between continuous fluid injection and progressive fracture propagation, thereby maintaining a steady and slow pressure reduction. ⑥ Secondary sharp pressure drop stage: As dominant fractures extend to the specimen boundaries, fluid leakage occurs, accompanied by reverse phase transition of $ScCO_2$. The resultant fluid vaporization and volume expansion further aggravate coal matrix damage and fracture dilation.

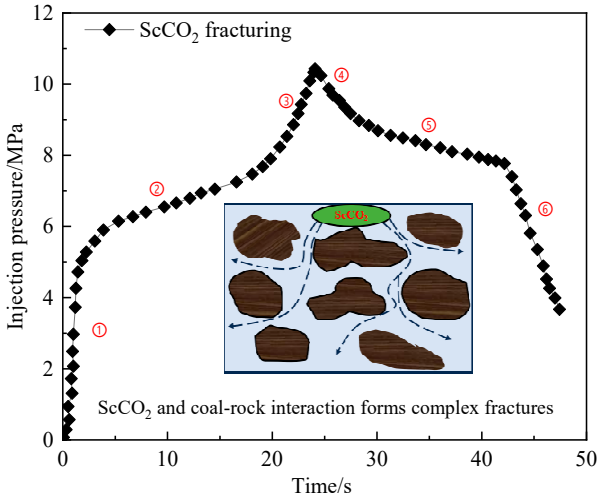


Figure 5. Complex fracture network formation mechanism of $ScCO_2$ fracturing. Arrows in the figure schematically represent $ScCO_2$ impingement on coal-rock media, fracture generation, and intrastratal fluid flow.

Experimental observations indicate that the fracture patterns induced by $ScCO_2$ fracturing are dominated by primary fractures propagating along the maximum principal stress orientation, with abundant deflected and branched secondary fractures. This phenomenon demonstrates the superior fracture networks construction capacity of $ScCO_2$ fracturing. The formation of complex fracture networks is governed by the synergistic coupling of $ScCO_2$ thermophysical behaviors, coal matrix heterogeneity, and multi-scale fluid–solid interactions. The low viscosity and zero surface tension of $ScCO_2$ enable the fluid to efficiently infiltrate micro- and nanopore throats, effectively elevating internal pore pressure and reducing the effective stress required for fracture initiation [29]. Near the critical point, CO_2 is susceptible to drastic phase and energy state variations, which accumulate substantial impact kinetic energy within fracture apertures. In addition, pervasive pre-existing microfractures and bedding planes in coal serve as inherent weak structural planes, providing favorable conditions for the development of complex fracture networks. When propagating main fractures encounter these discontinuities, tensile-shear composite failure and fracture deflection readily occur, generating dense secondary fracture branches [30]. Furthermore, CO_2 induces alterations in coal mechanical properties via physicochemical interactions, further weakening coal structural integrity. Overall, the multistage coupled effects of $ScCO_2$ infiltration, rapid pressurization, and post-fracturing expansion burst ultimately drive the formation of highly complex fracture networks in coal reservoirs [21,23,31].

3.2. $Scco_2$ Enhanced Gas Recovery

As illustrated in Figure 6, coal permeability undergoes a significant enhancement after saturation with $ScCO_2$ and formation water under high-temperature and high-pressure conditions. After 15 days of $ScCO_2$–formation water interaction treatment, coal permeability increases from 0.12×10^{-3} μm^2 to 0.31×10^{-3} μm^2, corresponding to an approximately 1.6-fold increment. Within the investigated experimental duration, the ultimate CH_4 recovery factor presents a positive correlation with soaking time. Specifically, the recovery factors for coal samples soaked for 0, 5, 10, and 15 days are 83.28%, 85.53%, 92.87%, and 93.85%, respectively. Notably, the coal sample subjected to 15 days of $ScCO_2$ soaking treatment achieves a 12.7% higher CH_4 recovery efficiency compared with the untreated counterpart.

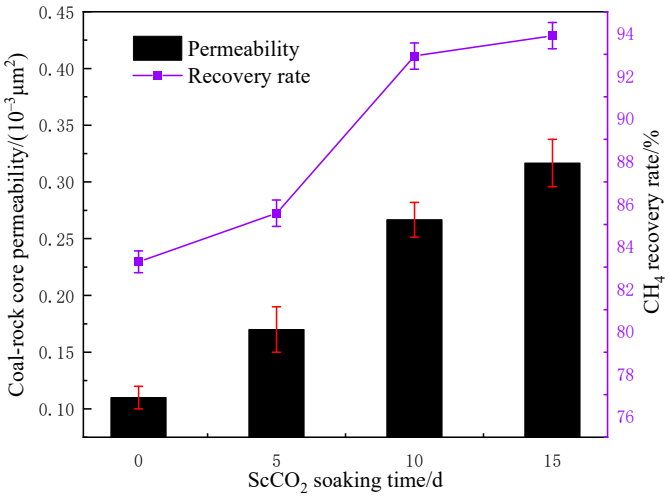


Figure 6. Core permeability and CH_4 recovery rate as a function of $ScCO_2$ treatment time.

Compared with shallow coalbed methane reservoirs, deep CRG reservoirs contain a relatively higher proportion of free gas, while adsorbed gas still dominates the total gas content, with free CH_4 generally accounting for less than 30% of the total gas volume in deep coal seams. Accordingly, the conversion of adsorbed CH_4 to free-state gas is regarded as a core mechanism for improving deep CRG recovery [32]. Previous studies have systematically confirmed the superior adsorption selectivity of CO_2 over CH_4 on coal matrices, based on variations in coal surface free energy during gas adsorption, thermodynamic characteristics of CO_2/CH_4 competitive adsorption, differences in molecular kinetic diameters, and the organic dissolution effect induced by $ScCO_2$. The adsorption capacity of coal for CO_2 is 2–10 times greater than that for CH_4, which serves as the fundamental mechanism for CO_2-induced CH_4 desorption and constitutes the primary principle for CO_2-enhanced CRG recovery [33,34].

3.3. Coal-Rock Mineral and Microstructural Changes

During CO_2 fracturing in CRG reservoirs, injected CO_2 reacts in situ with inherent seam water to form weak carbonic acid, which further dissolves and etches inorganic mineral components within the coal matrix. As demonstrated in Figure 7, prolonged supercritical CO_2–water interaction induces prominent dissolution of major carbonate and aluminosilicate minerals, including calcite, siderite, and anorthite. The elevated relative quartz content is primarily attributed to the dissolution and structural decomposition of clay minerals (i.e., kaolinite and illite), and the corresponding chemical reactions are defined in Equations (2)–(6).

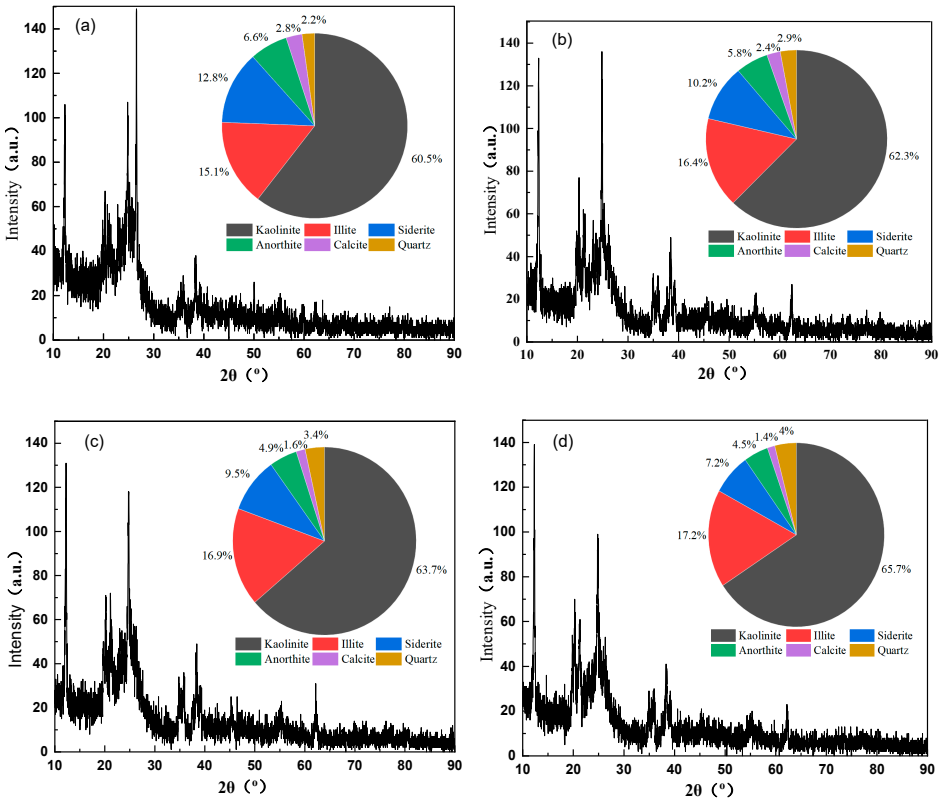


Figure 7. XRD patterns and relative mineral composition of coal rock treated with different $ScCO_2$ soaking times, (**a**) 0 d, (**b**) 5 d, (**c**) 10 d, (**d**) 15 d.

Quantitative mineralogical results reveal significant mineral degradation after 15 days of $ScCO_2$–water treatment. The relative content of calcite declines from 2.8% to 1.4%, representing a 50% reduction. Similarly, siderite decreases from 12.8% to 7.2% (43.8% reduction), and anorthite drops from 6.6% to 4.5% (31.8% reduction). Despite partial dissolution of clay minerals, the overall relative abundance of kaolinite and illite increases after the reaction. This variation indicates that, under high-temperature and high-pressure conditions, $ScCO_2$–aqueous fluid preferentially reacts with calcite, siderite, and anorthite, while the dissolution of clay minerals is relatively insignificant and subordinate.

$$Al_2SiO_5(OH)_4(\text{Kaolinite}) + 6H^+ = 2Al^{3+} + 2H_4SiO_4 + H_2O \quad (2)$$

$$KAl_2(Si_3Al)O_{10}(OH)_2(\text{Illite}) + 10H^+ = K^+ + 3Al^{3+} + 3SiO_2 + 6H_2O \quad (3)$$

$$CaCO_3(\text{Calcite}) + CO_2 + H_2O = Ca^{2+} + 2HCO_3^- \quad (4)$$

$$FeCO_3(\text{Siderite}) + H_2O + CO_2 = Fe^{2+} + 2HCO_3^- \quad (5)$$

$$CaAl_2Si_2O_8(\text{Anorthite}) + 3H_2O + 2CO_2 = Al_2SiO_5(OH)_4(\text{Kaolinite}) + Ca^{2+} + 2HCO_3^- \quad (6)$$

Figure 8 compares the Fourier-transform infrared (FTIR) spectra of raw and $ScCO_2$-treated coal specimens. The broad absorption band ranging from 3000 cm^{-1} to 3600 cm^{-1} is assigned to hydroxyl functional groups, which can be subdivided into six types of hydrogen bonds: OH–N hydrogen bonds (approximately 3150 cm^{-1}), cyclic hydrogen bonds (approximately 3200 cm^{-1}), OH–OR hydrogen bonds (approximately 3300 cm^{-1}), self-associated OH–OH hydrogen bonds (approximately 3410 cm^{-1}), OH–π hydrogen bonds (3516 cm^{-1}), and free OH bonds (3611 cm^{-1}) [35]. After $ScCO_2$ soaking, the relative contents of OH–N and OH–π hydrogen bonds decrease evidently, while other types of hydrogen bonds exhibit negligible variations in abundance. The spectral region of

1000–1800 cm^{-1} primarily corresponds to oxygen-containing functional groups in coal matrices. $ScCO_2$ treatment induces an apparent reduction in the contents of aliphatic ether, aromatic ether, aromatic C=C, carbonyl C=O, and carboxyl–COOH groups. In the low wavenumber range of 400–1500 cm^{-1}, the vibration intensities of CH_3, CH_2, C–O–C, and CH functional groups are also weakened after long-term $ScCO_2$ soaking [36]. Collectively, these spectral variations verify that $ScCO_2$ soaking disrupts the macromolecular functional group structures of coal and dissolves inherent small-molecule organic substances. Such structural modification effectively optimizes the pore system, thereby exerting a positive effect on improving coal porosity and permeability.

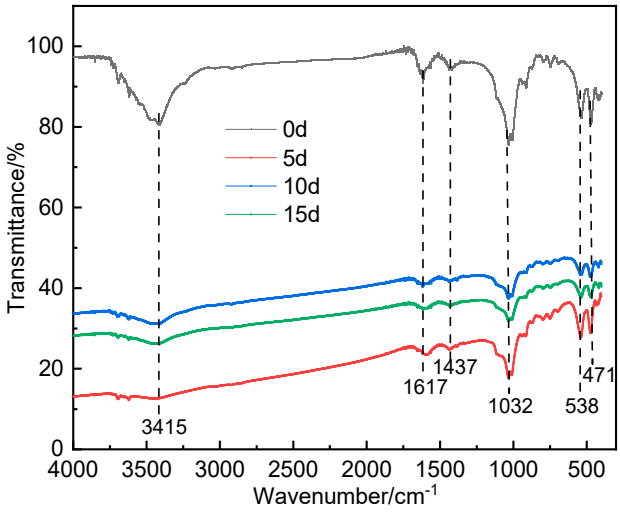


Figure 8. Infrared spectra of coal samples after different durations of $ScCO_2$ soaking.

Figure 9 illustrates the microstructural morphologies of coal specimens with different $ScCO_2$ soaking durations obtained by SEM. The raw untreated coal sample exhibits a relatively flat and intact surface, which is dominated by densely distributed micro- and nanopores with no evident macroscopic structural defects (Figure 9a). In contrast, significant micro-morphological variations are observed in coal after high-temperature and high-pressure $ScCO_2$–formation water–coal interactions. After five days of $ScCO_2$ treatment, the coal surface becomes considerably rougher, accompanied by a notable increase in both pore quantity and pore diameter (Figure 9b). This phenomenon demonstrates that the coupled hydro-chemical effects of $ScCO_2$ alter the inherent organic and mineral structures of coal, thereby reconstructing its intrinsic pore system. With the treatment duration extended to 10–15 days, the coal microstructure undergoes further dramatic modification (Figure 9c,d). Extensive large-scale fractures with widths exceeding 10 μm are generated on the coal surface, forming an interconnected preliminary fracture network and substantially expanding the reservoir seepage pathways.

Such microstructural evolution is highly consistent with the improved macroscopic permeability of treated coal. The $ScCO_2$–water coupling reaction enhances coal permeability by approximately 1.6 times, which verifies that $ScCO_2$ treatment effectively promotes the initiation, propagation and interconnection of coal micropores and microfractures. The reconstructed pore-fracture system significantly improves pore connectivity and seepage capacity of coal reservoirs. From the perspective of field application, a shut-in period of 10–15 days is recommended after $ScCO_2$ fracturing operations. This engineered shut-in strategy can fully exploit the pore dilation and permeability enhancement effects induced by sustained $ScCO_2$–water–coal interactions, so as to maximize the stimulation performance of coal reservoirs.

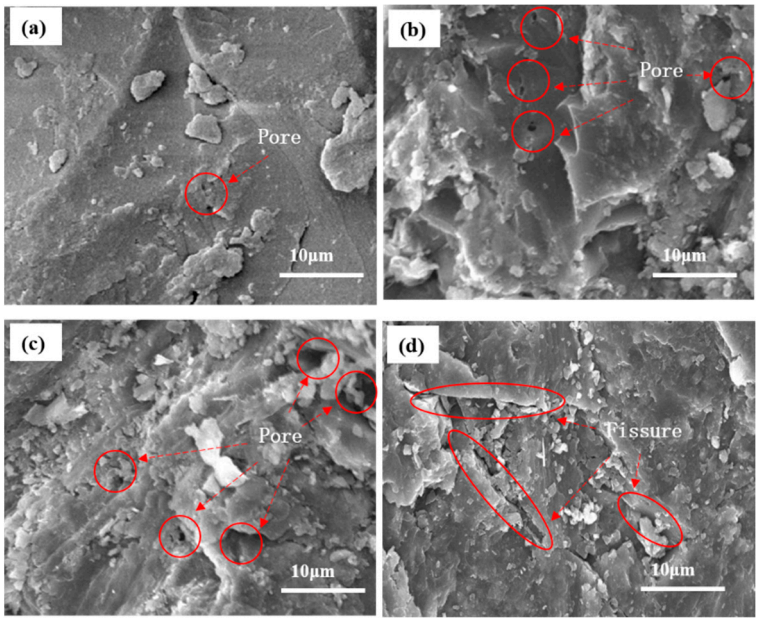


Figure 9. SEM images of coal samples after different durations of $ScCO_2$ soaking, (**a**) 0 d, (**b**) 5 d, (**c**) 10 d, (**d**) 15 d.

3.4. Analysis of the Mechanism for Increasing CRG Production Through $ScCO_2$ Fracturing

Based on the above experimental and microscopic analyses, the coalbed gas enhancement mechanisms associated with $ScCO_2$ fracturing can be comprehensively summarized into the following three aspects.

(1) Dynamic fracturing and complex fracture network generation. Compared with conventional hydraulic fracturing, $ScCO_2$ fracturing reduces coal breakdown pressure by 26.2% and shortens the fracture initiation time by 37.5%, demonstrating its superior capacity to induce coal matrix failure. Different from the single, simple fracture geometry formed by hydraulic fracturing, $ScCO_2$ fracturing creates penetrating primary fractures accompanied by abundant branched secondary fractures, thereby constructing a highly complex fracture network. The substantially improved fracture complexity provides a fundamental structural basis for efficient coalbed gas extraction during $ScCO_2$ fracturing stimulation.

(2) Coal matrix pore reconstruction and permeability enhancement. Raw coal is dominated by organic components and widely developed nanopore systems. A large proportion of semi-closed pores in pristine coal results in poor pore connectivity and low matrix permeability. The coupled $ScCO_2$–water interaction not only dissolves inorganic minerals within coal, but also disrupts organic functional groups via solvent extraction and molecular collision effects. These modifications transform original micropores into meso- and macropores and generate new pore-fracture seepage pathways, which significantly expand reservoir flow space. The reconstructed pore system provides sufficient adsorption sites for injected CO_2 and creates favorable hydrodynamic conditions for CO_2-driven CH_4 displacement [37].

(3) CO_2/CH_4 competitive adsorption and gas displacement effect. Coal matrices exhibit considerably higher adsorption selectivity and capacity for CO_2 than for CH_4, with the CO_2 adsorption magnitude 2–10 times greater than that of CH_4. This intrinsic adsorption discrepancy dominates CO_2-induced CH_4 desorption and serves as a core mechanism for improving coalbed gas recovery efficiency. During the displacement process, competitive gas adsorption and desorption occur simultaneously with multi-scale gas diffusion and seepage within the coal pore-fracture network. Relative to CO_2, CH_4 possesses weaker

adsorption affinity but a larger diffusion coefficient, enabling CO_2 to migrate in a typical piston-like displacement pattern. As illustrated in Figure 10, the entire displacement region can be divided into three distinct zones: a pure CO_2 single-phase zone, a CO_2–CH_4 binary miscible zone, and a residual CH_4 single-phase zone [38]. After CO_2 injection, free-phase CH_4 is rapidly displaced under pressure gradients, while adsorbed CH_4 gradually desorbs and migrates out of the coal matrix. Continuous CO_2 injection further promotes preferential CO_2 adsorption and sustained CH_4 desorption, ultimately achieving a prominent improvement in coalbed gas recovery.

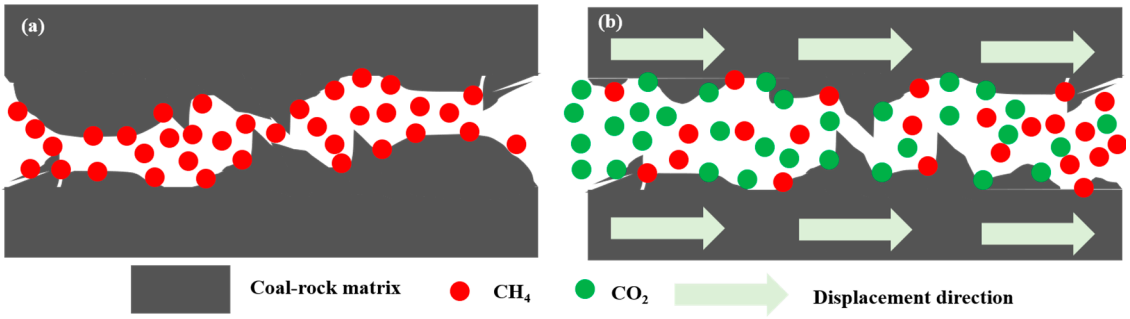


Figure 10. Schematic diagram of CO_2-CH_4 displacement mechanism, (**a**) original coal sample, (**b**) after soaking in SC-CO_2.

3.5. Field Application Case

(1) Overview of Geological Background and Reservoir Characteristics

The field test site is located in the Ordos Basin, a typical superimposed cratonic basin with abundant CRG resources hosted within the Carboniferous-Permian Benxi Formation. The target No. 8 coal seam reservoir developed stable sedimentary facies dominated by tidal flat and delta front deposits, featuring thin interbeds of coal, mudstone, and tight sandstone with widespread lateral continuity across the study block. Regional tectonic activity in this area is relatively weak, with low fault density and gentle formation dip angles, which avoids severe structural fragmentation and provides favorable geological conditions for large-scale fracturing reconstruction and long-term gas production monitoring.

Core petrophysical characterization of the No. 8 Benxi Formation reservoir reveals typical tight coal-rock reservoir properties: the coal matrix exhibits low intrinsic permeability ranging from 0.01 to 0.5 mD, limited natural fracture development, and high water sensitivity. Conventional water-based hydraulic fracturing tends to trigger water trapping and clay swelling within pore-fracture networks, severely damaging gas seepage channels and suppressing long-term gas deliverability. In contrast, supercritical carbon dioxide ($ScCO_2$) possesses unique advantages including low interfacial tension with coal surfaces, strong adsorption competitive capacity against methane, and zero water-phase damage, rendering it a promising alternative fracturing medium for water-sensitive coal measure reservoirs.

Two horizontal production wells within the same well block, namely Well SC-1 and adjacent contrast Well SW-1, were selected for controlled comparative field trials to quantitatively quantify the stimulation efficacy of $ScCO_2$ fracturing versus conventional hydraulic fracturing. Both wells target the identical No. 8 Benxi Formation coal-rock reservoir, with consistent burial depth range, in situ stress state, coal thickness, and original gas content, eliminating geological heterogeneity interference and ensuring the comparability of post-fracturing production responses.

(2) Well Completion and Fracturing Operation Design and Monitoring Scheme

Well SC-1 was deployed for supercritical CO_2 composite fracturing treatment, while the neighboring Well SW-1 adopted standard water-based hydraulic fracturing as the

reference baseline. Detailed well completion geometric parameters are documented as follows: the total measured depth of Well SC-1 reaches 4520 m with a 1130 m horizontal section extending along the strike of the coal seam; Well SW-1 features a total drilling depth of 4550 m and a 1095 m horizontal lateral segment. Both horizontal wells were divided into 13 independent fracturing stages with identical perforation cluster spacing and stage segmentation principles, maintaining uniform fracturing scale and reservoir coverage baseline for cross-method comparison.

Real-time dynamic monitoring systems were deployed throughout the full fracturing construction cycle to capture multi-dimensional operation data. Monitored parameters covered injection fluid displacement, cumulative injection volume of $ScCO_2$ and water-based fracturing fluid, proppant pumping rate, total sand loading, wellhead injection pressure, and downhole temperature evolution. For the $ScCO_2$ fracturing Well SC-1, the liquid CO_2 injection displacement was maintained at 4–6 $m^3 \cdot min^{-1}$, with auxiliary water-based carrier fluid displacement controlled within 6–12 $m^3 \cdot min^{-1}$ to stabilize underground supercritical phase transformation. The cumulative injected volume of pure CO_2 for SC-1 reached 5315 m^3, supplemented by 9714 m^3 of low-concentration water-based carrying fluid and 2223 m^3 of quartz sand proppant.

For contrast Well SW-1 adopting conventional hydraulic fracturing, no CO_2 injection was involved, and the water-based fracturing fluid displacement was elevated to 10–18 $m^3 \cdot min^{-1}$ to satisfy fracture propagation requirements. The total consumed water-based fluid volume surged to 30,269 m^3, with a total proppant sand dosage of 2608 m^3 across all 13 fracturing segments.

(3) Post-Fracturing Production Monitoring and Comparative Analysis

Continuous daily gas production monitoring was implemented for both wells over a consistent 90-day stable production period after fracturing shut-in and flowback operations, with daily gas output, water flowback volume, and bottom-hole flowing pressure recorded synchronously to characterize long-term reservoir stimulation performance. Field measurement and statistical analysis of fracture geometry and sweep range demonstrate remarkable disparities between the two reconstruction technologies.

Relative to conventional hydraulic fracturing applied in Well SW-1, $ScCO_2$ fracturing in Well SC-1 delivers a 6.7% increase in average effective fracture length, which originates from the low-viscosity property of supercritical CO_2 that facilitates deep penetration into micro-fractures within coal matrix. Meanwhile, the average fluid sweep area per fracturing stage is elevated by 10.9%, indicating that $ScCO_2$ can activate more microscale pore-fracture systems and expand the effective gas drainage volume of the coal reservoir.

In terms of production efficiency and water resource consumption, the average daily coal-rock gas output of Well SC-1 stabilized at 8.12×10^4 $m^3 \cdot d^{-1}$, approximately 20% higher than the 6.75×10^4 $m^3 \cdot d^{-1}$ gas production of the hydraulic fracturing well SW-1 under equivalent reservoir and completion conditions. More importantly, the adoption of $ScCO_2$ as the primary fracturing medium drastically cuts down water resource consumption: the total volume of water-based fluid utilized for SC-1 is merely 32.1% of that for SW-1, corresponding to a 67.9% reduction in fracturing water usage. This prominent advantage effectively mitigates water scarcity risks in arid Ordos Basin and eliminates formation damage induced by water retention and clay hydration swelling in tight coal reservoirs.

(4) Mechanism Implication of Field Test Results

The integrated field comparison results verify the dual benefits of $ScCO_2$ fracturing in coal-rock gas reservoirs: on one hand, supercritical CO_2 improves fracture propagation scale and expands the stimulated reservoir volume to boost methane recovery efficiency; on the other hand, it drastically reduces freshwater injection and avoids water-sensitive

reservoir damage. Beyond production enhancement, injected CO_2 can be stably adsorbed onto coal matrix surfaces for long-term geological sequestration, simultaneously realizing coal-rock gas-enhanced recovery and greenhouse gas geological storage, which provides a technical reference for low-carbon, water-saving reservoir reconstruction in similar tight coal-bearing basins worldwide.

4. Discussion of Experimental Limitations and Upscaling Uncertainties for Field Implementation

Although the multi-scale laboratory experiments combining true triaxial fracturing, CO_2–CH_4 competitive displacement and microscale spectroscopic characterizations (XRD, FTIR, SEM) adequately reveal the intrinsic coupled mechanisms of $ScCO_2$ fracturing for enhanced coal-rock gas recovery under controlled boundary conditions, the experimental design and specimen scale inevitably contain inherent simplifications that deviate from the complex geological and engineering realities of in situ coal reservoirs. Such discrepancies introduce non-negligible uncertainties when extrapolating laboratory-derived quantitative laws, characteristic parameters and mechanistic understandings to full-scale field operations, which are elaborated systematically below.

4.1. Inherent Limitations of Laboratory Experimental Settings

First, the geometric scale and integrity of coal specimens create prominent scale effects. All laboratory tests rely on intact small-scale coal blocks without widespread natural fracture networks, tectonic fissures, interlayer mudstone barriers, and vertical stratification interfaces that universally exist in actual coal-rock strata. In field formations, multi-scale natural fractures serve as primary channels for $ScCO_2$ penetration and hydro-chemical reactions, while lab samples only contain limited microcracks formed during coring and processing. Consequently, the measured breakdown pressure, fracture propagation morphology and permeability amplification magnitude obtained in laboratory environments cannot fully replicate the fracture activation behaviors of heterogeneous, fractured in situ coal seams. In addition, the soaking duration adopted in this work is restricted to 15 days, which only captures short-term mineral dissolution and pore reconstruction responses. Long-term geochemical water–$ScCO_2$–coal interactions spanning months to years underground may induce secondary mineral precipitation, pore blockage and irreversible matrix deformation—such long-term evolutionary processes are not captured within the current experimental framework, leading to incomplete evaluation of sustained reservoir permeability evolution.

Second, simplified boundary and environmental conditions narrow the representativeness of experimental outcomes. The true triaxial test system applies uniform, static in situ stress fields with fixed temperature and constant $ScCO_2$ injection rates throughout fracturing and soaking stages. In subsurface reservoirs, however, stress gradients fluctuate drastically along horizontal wellbores and fracturing segments, accompanied by dynamic temperature variations during $ScCO_2$ phase transition, heterogeneous formation water salinity and uneven clay mineral distribution. High-salinity formation brine in real coal seams may alter mineral dissolution rates and weaken the competitive adsorption advantage of CO_2 over CH_4, whereas deionized water adopted in lab tests eliminates ionic interference, overestimating the permeability-improving efficiency of $ScCO_2$ treatment to a certain extent. Moreover, the displacement experiments are conducted under closed isothermal adsorption cells without considering dynamic gas seepage pressure attenuation and multi-phase flow coupling of $ScCO_2$, methane and formation water, which simplifies the actual multiphase transport process within stimulated reservoir volumes.

Third, artificial coal sample preparation introduces artificial damage deviating from native reservoir matrices. Coring, cutting and polishing inevitably generate artificial microcracks on specimen surfaces, which reduce the measured fracture initiation threshold and accelerate hydro-chemical erosion compared with undisturbed in situ coal. Meanwhile, the laboratory excludes engineering interference factors widely encountered in field construction, including proppant transport, near-wellbore fracture tortuosity, wellbore pollution, and non-uniform $ScCO_2$ distribution across multiple fracturing stages. These omitted engineering variables make the lab-measured ultimate methane recovery factor (93.85%) an ideal upper-limit value that is difficult to reproduce under actual field production conditions.

4.2. Key Uncertainties in Upscaling Laboratory Mechanisms to Field Applications

The quantitative relationships and core coupled mechanisms identified from lab-scale characterization face multiple transformation uncertainties when extended to full-scale $ScCO_2$ fracturing field treatments, primarily originating from geological heterogeneity, engineering construction differences and long-term reservoir dynamic evolution.

(1) Uncertainty in fracture network propagation and stimulated reservoir volume (SRV) upscaling

The complex fracture networks observed in true triaxial lab specimens form under uniform stress and homogeneous coal matrices, yet subsurface coal reservoirs feature strong lateral heterogeneity in coal thickness, gas content, rock mechanical strength and natural fracture density. Under identical $ScCO_2$ injection parameters, areas with well-developed natural fractures tend to form large-scale complex fracture networks, while tight intact coal zones only generate single planar fractures. The 26.2% reduction in breakdown pressure and 6.7% extension of effective fracture length obtained from lab comparative tests cannot be directly applied to predict field fracture geometry, as interlayer interfaces and fault structures may restrain vertical fracture propagation or trigger unexpected fracture height migration, altering the overall SRV morphology and effective gas drainage range.

(2) Uncertainty in long-term permeability evolution driven by subsurface geochemical reactions

Laboratory observations confirm that 15-day $ScCO_2$ soaking dissolves calcite, plagioclase and clay minerals to enlarge pore throats and lift permeability by 1.6 times. Nevertheless, deep coal reservoirs contain complex mixed brine with variable ion concentrations, which may trigger secondary carbonate precipitation after prolonged $ScCO_2$ injection, partially plugging newly generated pore throats and offsetting permeability enhancement effects. In addition, long-term in situ stress creep deformation of coal matrices compresses micro-pores and fractures over production cycles, further complicating the long-term permeability evolution trend. The short-term lab experimental window fails to quantify the balance between mineral dissolution and pore compaction/precipitation, introducing significant uncertainty in predicting sustained reservoir deliverability after field $ScCO_2$ stimulation.

(3) Uncertainty in competitive adsorption and actual field methane recovery potential

The 93.85% ultimate CH_4 recovery factor measured via laboratory displacement tests represents an ideal state with sufficient $ScCO_2$ supply and full contact between CO_2 and coal matrix adsorption sites. In field practice, $ScCO_2$ is unevenly distributed within the fracture network, and large portions of the coal matrix remain inaccessible to injected CO_2 due to flow barriers. Additionally, desorbed methane may be re-adsorbed by unreacted coal under varying bottom-hole flowing pressure during production, lowering the effective recovery efficiency compared with lab measurements. The 12.7% recovery improvement over

untreated coal samples derived from laboratory comparison thus serves as an optimistic theoretical benchmark rather than a guaranteed field production increment.

(4) Engineering and carbon sequestration coupling uncertainties under field operation constraints

Laboratory tests separate fracturing injection, $ScCO_2$ soaking and gas displacement into independent stages for controlled analysis, whereas field construction integrates continuous $ScCO_2$ pumping, flowback and long-term production. Variable pump displacement, proppant clogging and near-wellbore phase transition loss reduce the effective volume of $ScCO_2$ entering deep reservoir matrices, weakening both reservoir modification and geological CO_2 storage capacity. Furthermore, the lab cannot replicate field-scale CO_2 leakage risks along wellbores and fracture boundaries, which complicates the comprehensive evaluation of the dual benefits of enhanced CRG recovery and greenhouse gas sequestration under real engineering scenarios.

4.3. Outlook for Mitigating Scale-Translation Limitations

To bridge the gap between lab-scale mechanistic research and field engineering practice, subsequent investigations should integrate numerical simulation and field monitoring data to correct the bias of laboratory experimental results. Multi-physics-coupled numerical models can incorporate reservoir heterogeneity, dynamic in situ stress evolution and long-term geochemical reactions to establish scale transformation correction formulas for lab-derived permeability, fracture and recovery parameters. Meanwhile, long-duration core flooding experiments lasting several months, combined with field microseismic fracture monitoring and real-time production data recording, will help quantify the long-term pore-fracture evolution law of coal reservoirs and narrow the uncertainty margins of upscaling prediction. Further field pilot tests with multi-well comparative monitoring are required to calibrate the three-core coupled $ScCO_2$ stimulation mechanisms proposed in this work, thereby providing more reliable quantitative guidance for large-scale green $ScCO_2$ fracturing exploitation of deep coal-rock gas.

5. Conclusions

In this work, the fundamental mechanisms of $ScCO_2$ fracturing for coal-rock gas (CRG) enhancement were systematically investigated via true triaxial fracturing experiments, CO_2–CH_4 displacement tests, and multi-scale microscopic characterization techniques, including XRD, FTIR, and SEM. The primary conclusions are summarized as follows:

(1) Under identical in situ stress, temperature, and injection rate conditions, $ScCO_2$ fracturing substantially reduces coal breakdown pressure by 26.2% and shortens fracture initiation duration by 37.5% relative to conventional hydraulic fracturing. Such superior fracturing performance facilitates the efficient activation of coal fractures and promotes the development of complex fracture networks within coal reservoirs.

(2) Long-term $ScCO_2$ soaking triggers intense hydro-chemical interactions with coal matrices, resulting in prominent dissolution of inorganic minerals (e.g., calcite, plagioclase, and clay minerals) and effective extraction of intrinsic organic matter. The coupled physicochemical reactions reconstruct the internal pore architecture, enlarge pore throats, and improve reservoir seepage capacity. After 15 days of $ScCO_2$ soaking, coal permeability is enhanced by approximately 1.6 times.

(3) $ScCO_2$ displacement exhibits excellent performance in improving CRG recovery. The ultimate CH_4 recovery factor reaches 93.85% for coal samples after 15 days of soaking, which is 12.7% higher than that of the untreated coal. Coal matrices possess a greater adsorption capacity for CO_2 than for CH_4, leading to prominent preferential CO_2 adsorption. This competitive adsorption effect serves as the core

mechanism for promoting the desorption of adsorbed methane and improving CRG recovery efficiency.

(4) The CRG enhancement mechanism of $ScCO_2$ fracturing is dominated by three synergistic coupled effects. First, dynamic $ScCO_2$ fracturing generates highly complex fracture networks, which greatly optimize reservoir seepage pathways. Second, sustained $ScCO_2$–formation water–coal interactions reconstruct coal pore structures and enhance matrix permeability via mineral dissolution and organic matter extraction. Third, CO_2-preferred competitive adsorption displaces adsorbed CH_4, further facilitating methane desorption and migration.

(5) This study clarifies the multi-scale modification and gas-stimulation mechanisms of $ScCO_2$ treatment in deep coal reservoirs. The findings provide a reliable theoretical basis for the field implementation of $ScCO_2$ fracturing technology and offer valuable guidance for the green, efficient, and sustainable exploitation of deep coal-rock gas resources.

(6) Although this laboratory investigation reveals the coupled mechanisms of $ScCO_2$ stimulation for coal-rock gas recovery, its results are constrained by inherent experimental simplifications and prominent upscaling uncertainties for field deployment. Key limitations include small intact coal specimens, a 15-day short reaction period, static uniform stress, and artificial sample damage, which collectively overestimate fracture propagation, permeability growth and methane recovery. Further uncertainties arise from subsurface geological heterogeneity, dynamic in situ stress, complex formation brine, multiphase flow and on-site engineering constraints, hindering accurate prediction of field fracture geometry, long-term reservoir performance and CO_2 sequestration efficiency. Future work will adopt multi-physics numerical models to establish lab-to-field scaling correlations, perform long-duration core flooding tests to capture long-term geochemical evolution, and conduct monitored multi-well field pilots to calibrate the proposed $ScCO_2$ stimulation mechanisms, supporting large-scale green exploitation of deep coal-rock gas.

Author Contributions: X.S.: Conceptualization, investigation, validation, formal analysis, data curation, writing—original draft preparation, writing—review and editing, resources; M.Z.: conceptualization, investigation, resources, writing—review and editing; Y.G.: investigation; H.X.: funding acquisition, investigation; Z.L.: investigation, formal analysis; J.Y.: formal analysis, data curation. All authors have read and agreed to the published version of the manuscript.

Funding: This research was funded by National Natural Science Foundation of China, under grant number 52374027.

Data Availability Statement: The original contributions presented in this study are included in the article. Further inquiries can be directed to the corresponding author.

Conflicts of Interest: All authors were employed by the Changqing Downhole Technology Operating Company, CNPC Chuanqing Drilling Engineering Co., Ltd. The authors declare that the research was conducted in the absence of any commercial or financial relationships that could be construed as a potential conflict of interest.

References

1. Zhang, J.; Li, G.; Jia, C.; Zhao, Q. Natural gas types and coal-rock gas classification in the whole petroleum system of coal measures. *Petrol. Explor. Dev.* **2025**, *52*, 894–906. [CrossRef]
2. Guo, Z.; Dong, C.; Wang, B.; Li, L.; Pang, Z.; Chen, X.; Ma, D. Geological characteristics of Jurassic coal rock gas and evaluation of favorable zones in the northern structural belt of the Kuqa Depression, Tarim Basin, China. *J. Nat. Gas GeoSci.* **2025**, *10*, 219–238. [CrossRef]

3. Liu, H.; Wang, H.; Deng, Z.; Huang, D. Accumulation characteristics and models of low-rank multi-source coal-rock gas in the Jurassic of Junggar Basin, China. *J. Nat. Gas GeoSci.* **2026**, *11*, 15–30. [CrossRef]
4. Li, G.; Chen, R.; Wen, Z.; Zhang, J.; He, Z.; Feng, J.; Kang, H.; Meng, Q.; Ma, C.; Su, L. Global coal-rock gas resource potential and distribution. *Petrol. Explor. Dev.* **2026**, *53*, 16–30. [CrossRef]
5. Niu, X.; Fan, L.; Yan, X.; Zhou, G.; Zhang, H.; Jing, X.; Zhang, M. Enrichment conditions and resource potential of coal-rock gas in Ordos Basin, NW China. *Petrol. Explor. Dev.* **2024**, *51*, 1122–1137. [CrossRef]
6. Li, C.; Yang, Z.; Yan, X.; Wang, G.; Huang, D.; Lu, B.; Zhang, B.; Feng, S.; Wang, J.; Liu, C.; et al. Dynamic distribution patterns and release behavior of adsorbed gas/free gas during deep coalbed methane production. *Fuel* **2026**, *407*, 137310. [CrossRef]
7. Zhang, B.; Tao, S.; Sun, B.; Tang, S.; Chen, S.; Wen, Y.; Ye, J. Genesis and accumulation mechanism of external gas in deep coal seams of the Baijiahai Uplift, Junggar Basin, China. *Int. J. Coal Geol.* **2024**, *286*, 104506. [CrossRef]
8. Si, S.; Kang, J.; Yang, X.; Zhang, R.; Guo, W. A parameter inversion method for coal seam gas pressure based on gas flow rate during drilling process. *Fuel* **2026**, *419*, 138803. [CrossRef]
9. Zhang, Z.; Zhu, J. Origins of Paleozoic natural gas in the Ordos Basin, North China, and implications for carbon isotope reversal mechanism. *Org. Geochem.* **2026**, *217*, 105198. [CrossRef]
10. Li, G.; Zhang, J.; Zhao, Q.; Chen, H.; Chen, Y.; Zhang, G.; Tian, W.; Wang, M.; Deng, Z.; Xu, W. Evaluation methodology of coal-rock gas resources and exploration potential of favorable areas in onshore China. *Petrol. Explor. Dev.* **2025**, *52*, 1389–1406. [CrossRef]
11. Yang, F.; Li, B.; Wang, K.; Wen, H.; Yang, R.; Huang, Z. Extreme massive hydraulic fracturing in deep coalbed methane horizontal wells: A case study of the Linxing Block, eastern Ordos Basin, NW China. *Petrol. Explor. Dev.* **2024**, *51*, 440–452. [CrossRef]
12. Li, H.; Alumur, S.A. Multi-period reverse logistics network design for water resource management in hydraulic fracturing. *Appl. Math. Model.* **2024**, *129*, 612–632. [CrossRef]
13. Shrestha, N.; Chilkoor, G.; Wilder, J.; Gadhamshetty, V.; Stone, J.J. Potential water resource impacts of hydraulic fracturing from unconventional oil production in the Bakken shale. *Water Res.* **2017**, *108*, 1–24. [CrossRef] [PubMed]
14. Hou, B.; Li, Z.; Yang, W.; Gao, Y.; Wang, Y.; Hao, Z. Impact of hydraulic fracturing combined with CO_2 gas injection displacement on coalbed methane extraction. *Int. J. Rock Mech. Min. Sci.* **2026**, *202*, 106491. [CrossRef]
15. Zhang, K.; Hou, Y.; Cao, H.; Wang, T.; Li, H.; Wang, T.; Zhang, X.; Niu, Y.; Qiu, G.; Wang, C. Eco-friendly utilization of oilfield fracturing flow-back fluid and coal pitch for preparing slurry: Experiments and extended DLVO study. *J. Petrol. Sci. Eng.* **2022**, *216*, 110786. [CrossRef]
16. Xie, Y.; Fan, X.; Zhou, C.; Wang, H.; Mao, Z.; Wang, B.; Mao, F.; Stanchits, S.; Cheremisin, A. Study on fracture initiation and expansion of coal rock by CO_2 foam fracturing. In Proceedings of the 58th U.S. Rock Mechanics/Geomechanics Symposium, Golden, CO, USA, 23–26 June 2024. [CrossRef]
17. Xu, J.; Zhai, C.; Liu, S.; Qin, L.; Sun, Y. Feasibility investigation of cryogenic effect from liquid carbon dioxide multi cycle fracturing technology in coalbed methane recovery. *Fuel* **2017**, *206*, 371–380. [CrossRef]
18. Karacan, C.Ö.; Ruiz, F.A.; Cotè, M.; Phipps, S. Coal mine methane: A review of capture and utilization practices with benefits to mining safety and to greenhouse gas reduction. *Int. J. Coal Geol.* **2011**, *86*, 121–156. [CrossRef]
19. Shang, Z.; Zhang, J.; Wang, H.; Wang, Z.; Li, B.; Guo, P.; Zhang, X. Fracture propagation characteristics driven by liquid CO_2 BLEVE for coalbed methane recovery. *Fuel* **2025**, *381*, 133162. [CrossRef]
20. Yang, Z.-Z.; Yi, L.-P.; Li, X.-G.; Chen, Y.-T.; Sun, J. Model for calculating the wellbore temperature and pressure during supercritical carbon dioxide fracturing in a coalbed methane well. *J. CO_2 Util.* **2018**, *26*, 602–611. [CrossRef]
21. Wang, X.; Pan, J.; Wang, H.; Tang, Z.; Wang, Z.; Li, Y.; Song, D. Transformation effect of multi-Scale pores induced by true triaxial supercritical carbon dioxide fracturing in high-rank coal. *Gas Sci. Eng.* **2025**, *139*, 205644. [CrossRef]
22. Leng, K.; Guan, B.; Jiang, C.; Liu, W. Integrated analysis of pore and fracture networks in deep coal seams: Implications for enhanced reservoir stimulation. *Energies* **2025**, *18*, 3235. [CrossRef]
23. Wang, X.; Pan, J.; Jin, Y.; Du, X.; Wang, Z.; Cheng, N.; Hou, Q. Morphology and propagation of supercritical carbon dioxide-induced fractures in coal based on a non-destructive surface extraction method. *Fuel* **2025**, *384*, 133948. [CrossRef]
24. Pan, J.; Du, X.; Wang, X.; Hou, Q.; Wang, Z.; Yi, J.; Li, M. Pore and permeability changes in coal induced by true triaxial supercritical carbon dioxide fracturing based on low-field nuclear magnetic resonance. *Energy* **2024**, *286*, 129492. [CrossRef]
25. Ma, H.; Yang, Y.; Xue, Z.; Clarkson, C.R.; Chen, Z. Transitioning from emission source to sink: Economic and environmental trade-offs for CO_2-enhanced coalbed methane recovery of Mannville coal Canada. *Sci. Total Environ.* **2025**, *966*, 178721. [CrossRef] [PubMed]
26. Torrik, A.; Rezaee, M.; Valadi, F.M. Theoretical investigation of CO_2/N_2-enhanced coalbed methane recovery in coal-derived asphaltenes. *Fuel* **2025**, *395*, 134693. [CrossRef]
27. Jeon, P.R.; Lee, H.-H.; Keffer, D.J.; Lee, C.-H. Statistical mechanic and machine learning approach for competitive adsorption of CO_2/CH_4 on coals and shales for CO_2-enhanced methane recovery. *Chem. Eng. J.* **2024**, *495*, 153200. [CrossRef]

28. Zhang, L.; Shan, Y. Quantitative analysis of fracture roughness and multi-field effects for CO_2-ECBM projects. *Energies* **2024**, *17*, 2851. [CrossRef]
29. Liu, X.; Nie, B.; Guo, K.; Zhang, C.; Wang, Z.; Wang, L. Permeability enhancement and porosity change of coal by liquid carbon dioxide phase change fracturing. *Eng. Geol.* **2021**, *287*, 106106. [CrossRef]
30. Xu, W.; Yu, H.; Zhang, J.; Lyu, C.; Wang, Q.; Micheal, M.; Wu, H. Phase-Field method of crack branching during SC-CO_2 fracturing: A new energy release rate criterion coupling pore pressure gradient. *Comput. Methods Appl. Mech. Eng.* **2022**, *399*, 115366. [CrossRef]
31. Yu, B.; Niu, S.; Zhou, S.; Lei, Y.; He, Z.; Luo, X. Impact pressure characteristics of carbon dioxide phase transition fracturing technique. *ACS Omega* **2024**, *9*, 23927–23939. [CrossRef] [PubMed]
32. Mastalerz, M.; Gluskoter, H.; Rupp, J. Carbon dioxide and methane sorption in high volatile bituminous coals from Indiana, USA. *Int. J. Coal Geol.* **2004**, *60*, 43–55. [CrossRef]
33. Sun, J.; Chen, Z.; Wang, X.; Zhang, Y.; Qin, Y.; Chen, C.; Li, W.; Zhou, W. Displacement characteristics of CO_2 to CH_4 in heterogeneous surface slit pores. *Energy Fuels* **2023**, *37*, 2926–2944. [CrossRef]
34. Xing, Y.; Jia, J. Thermodynamics and diffusion mechanism of competitive adsorption of CH_4, CO_2 and N_2 in different coal slit pores. *Colloids Surf. A* **2025**, *726*, 137943. [CrossRef]
35. Van Niekerk, D.; Pugmire, R.J.; Solum, M.S.; Painter, P.C.; Mathews, J.P. Structural characterization of vitrinite-rich and inertinite-rich Permian-aged South African bituminous coals. *Int. J. Coal Geol.* **2008**, *76*, 290–300. [CrossRef]
36. Li, R.; Ge, Z.; Wang, Z.; Zhou, Z.; Zhou, J.; Li, C. Effect of supercritical carbon dioxide ($ScCO_2$) on the microstructure of bituminous coal with different moisture contents in the process of $ScCO_2$ enhanced coalbed methane and CO_2 geological sequestration. *Energy Fuels* **2022**, *36*, 3680–3694. [CrossRef]
37. Niu, Q.; Li, S.; Wang, W.; Sang, S.; Liu, S.; Liu, D.; Han, S.; Liu, T.; Zheng, S. Dynamic fracture behavior and permeability response mechanism of coal reservoirs treated by supercritical CO_2 and water: Implications for safety evaluation of CO_2 geological sequestration in coal seams. *Eng. Fail. Anal.* **2026**, *191*, 110774. [CrossRef]
38. Fang, Z.; Yang, C.; Shen, S. Experimental investigation of CO_2-enhanced coalbed methane recovery using large intact coal cores. *J. CO_2 Util.* **2025**, *100*, 103185. [CrossRef]

Disclaimer/Publisher's Note: The statements, opinions and data contained in all publications are solely those of the individual author(s) and contributor(s) and not of MDPI and/or the editor(s). MDPI and/or the editor(s) disclaim responsibility for any injury to people or property resulting from any ideas, methods, instructions or products referred to in the content.